The Biotic–Thermal Vapor Pump: A Phased, Transboundary Framework for Salton Sea Dust Remediation and Critical-Mineral Recovery through Brine-Free Solar-Thermal Evaporation, Halophytic Silviculture, and Closed-Loop Geothermal Energy

Brent Hartshorn

June 4, 2026

Abstract

This paper introduces a phased, transboundary framework for arresting the public-health dust hazard of the desiccating Salton Sea while recovering critical minerals from imported marine water. Decades of "Sea-to-Sea" proposals to import water from the Gulf of California have foundered on three obstacles repeatedly identified by independent state review: tens of billions of dollars in cost, multi-decade timelines, and the ecological damage of discharging concentrated brine back into the Gulf. We propose the "Biotic–Thermal Vapor Pump" (BTVP), sited in the below-sea-level Laguna Salada basin of Baja California, Mexico, whose central innovation directly removes the brine-discharge obstacle. Phase I couples a scale-asymmetric halophytic canopy (*Avicennia germinans* and *Rhizophora mangle*) to a recently demonstrated additive-free, brine-discharge-free solar-thermal evaporator (laser-textured superwicking black metal) that recovers nearly all dissolved salts—and, via embedded hydrogen-titanate nanoparticles, lithium—as solid product rather than as toxic concentrate, converting the terminal-basin salt-disposal liability into a managed resource stream. Phase II incorporates deep, closed-loop downhole heat exchangers to safely tap the underlying 187°C geothermal reservoir without phreatomagmatic or halite-hydrolysis hazard, and to access the lithium-rich (∼100–300 mg/L) native geothermal brine of the "Lithium Valley" resource. Phase III integrates a DNA-inspired pyrimidone Molecular Solar Thermal (MOST) matrix as a timing actuator for on-demand vapor pulses. We present coupled mass, salinity, thermodynamic, and atmospheric models, and—critically—bound each subsystem against the relevant physics. The dominant, defensible benefits are dust suppression, brine-free salinity management, and critical-mineral recovery; we show by moisture-budget and recycling-ratio analysis that the local atmospheric contribution to downwind precipitation is a small, bounded effect rather than a primary water-supply mechanism, and we present it as such. Finally, we frame the design as Stage 1 of a two-stage program: an independently beneficial Mexican-basin installation that proves the brine-free zero-liquid-discharge desalination chain and thereby makes credible a Stage 2 in which the same technology—answering the decisive brine-discharge objection that ended prior state review of Gulf importation—enables direct stabilization of the Salton Sea itself.

1 Introduction

The progressive desiccation of the Salton Sea represents one of the most acute environmental and public health crises in North America. As the water level declines, thousands of acres of exposed terminal lake bed—or playa—are subjected to intense desert winds, generating severe dust storms. This playa does not consist of inert sediment; it contains highly concentrated concentrations of arsenic, lead, pesticides, and municipal agricultural runoff, effectively qualifying the dust as a toxic hazard that causes severe respiratory distress in surrounding populations. Conventional dust mitigation strategies remain prohibitively expensive and logistically challenging to scale across the expanding basin floor. To resolve this crisis, "Sea-to-Sea" import proposals have been advanced for more than three decades, in which marine water is conveyed from the Gulf of California (or the Pacific) to stabilize the lake surface and manage its salinity [1]. In May 2021 the State of California's Salton Sea Management Program [3] commissioned the University of California

Santa Cruz to evaluate such concepts, and an Independent Review Panel reviewed eighteen public water-importation submissions, most of which envisioned drawing Gulf of California water, desalinating it, and conveying it north by canal [2]. A gulf route is attractive because the Laguna Salada basin lies below sea level, requiring comparatively modest lift, but it requires a new bilateral treaty with Mexico. In its September 2022 summary report, the Panel narrowed the eighteen concepts to three on the basis of fatal flaws, analyzed those alongside two additional approaches it identified, and concluded that none of the importation concepts was feasible or recommended [2]. The decisive objections were capital costs in the tens of billions of dollars, construction timelines exceeding twenty years, and—for the environmental case—the damage of discharging tens of millions of tons of concentrated brine back into the sensitive Gulf of California ecosystem. Notably, several submitted concepts already anticipated elements of an integrated approach, including mangrove-based filtration, desalination, and coupling to geothermal plants [1]; the framework developed here can be read as a physically constrained synthesis of that family of ideas, with the brine-discharge obstacle removed by design.

A recurring structural assumption in the most ambitious of these concepts is that marine water conveyed into the naturally below-sea-level Laguna Salada basin could be evaporated under the region's extreme summer temperatures, with the resulting moisture carried north-northwest toward the Chocolate, Cottonwood, and Santa Rosa ranges to fall as orographic precipitation within the Salton Sea watershed. As we show quantitatively in Section 2.3, this atmospheric "pump-and-rain" mechanism cannot serve as a primary water-supply pathway: the local vapor source is a sub-percent perturbation on the synoptic moisture flux, and standard recycling-ratio physics bounds the in-region precipitation return one to two orders of magnitude below the volumes such concepts have assumed. We therefore retain the managed-evaporation architecture for what it can defensibly deliver—brine-free salinity control, dust suppression, critical-mineral recovery, and bounded local humidity modification—rather than as a rain-making engine. However, open-surface mechanical proposals exhibit critical thermodynamic, geochemical, and volcanological vulnerabilities:

- The Hypersalinity Evaporation Limit: Continuous unbuffered seawater influx into a terminal basin rapidly generates a hypersaline brine. As salt concentrations approach saturation, the chemical activity of water (a_w) drops precipitously according to Raoult's Law, suppressing the vapor pressure and shutting down the evaporative loop while introducing a secondary toxic playa footprint within Mexico.

- Hydrovolcanic and Corrosive Hazards: Direct injection of marine fluids into an open magmatic heat source to generate steam risks causing destructive phreatomagmatic or phreatic eruptions due to rapid volumetric steam expansion. Furthermore, high-temperature direct contact between seawater and molten silicates triggers the hydrolysis of halite, generating high-volume plumes of volatile, highly corrosive hydrochloric acid (HCl) gas.

- Atmospheric Venting and Convective Inhibition: Arbitrary, uncoordinated moisture injection into the planetary boundary layer (PBL) can fail to breach the local convective inhibition (CIN) layer imposed by the subtropical high-pressure belt, leading to non-localized advection or simple elevations of the regional heat index without generating orographic rain.

To resolve these structural flaws, this paper establishes a practical, mathematically constrained engineering proposal. We replace the raw mechanical evaporation pool with a phased biological and advanced material system. First, large-scale halophytic tree planting (Mangroves) is deployed as a nature-based geoengineering sink to stabilize soil moisture, trap dust, prevent unmanaged salt pans, and lift subsurface water into the atmosphere via controlled transpiration [4] [5] [6]. This biotic layer is paired with an engineered evaporation layer based on a 2026 University of Rochester breakthrough [12] [14]: an additive-free, brine-discharge-free solar-thermal desalination architecture using femtosecond-laser-textured superwicking black metal. By exploiting microscopic groove patterning and the coffee-ring effect to continuously advect crystallizing salts away from the active evaporation zone toward passive collection regions, this surface directly defeats the hypersalinity scaling and crusting (magnesium/calcium hard scale) that otherwise terminates open-surface evaporation, and it recovers nearly all dissolved solids—including, via embedded hydrogen-titanate nanoparticles, lithium [13]—as solid product rather than toxic brine. Second, to exploit the massive energy potential observed in deep-sea eruptions and sub-benthic reservoirs without explosive risk, we replace open-cycle systems with strictly isolated, binary closed-loop downhole heat exchangers [7]. Third, we integrate a 2026

breakthrough from UC Santa Barbara and UCLA [8] [9] [10] [11]: a DNA-inspired, pyrimidone-based Molecular Solar Thermal (MOST) material capable of absorbing solar energy, storing it indefinitely within stable chemical bonds, and releasing it as intense heat via a localized catalyst on demand. This enables temporal control over vapor generation, aligning moisture injection with dynamic meteorological windows to maximize precipitation efficiency as governed by satellite-validated atmospheric scaling laws.

2 Mathematical Framework and Predictive Modeling

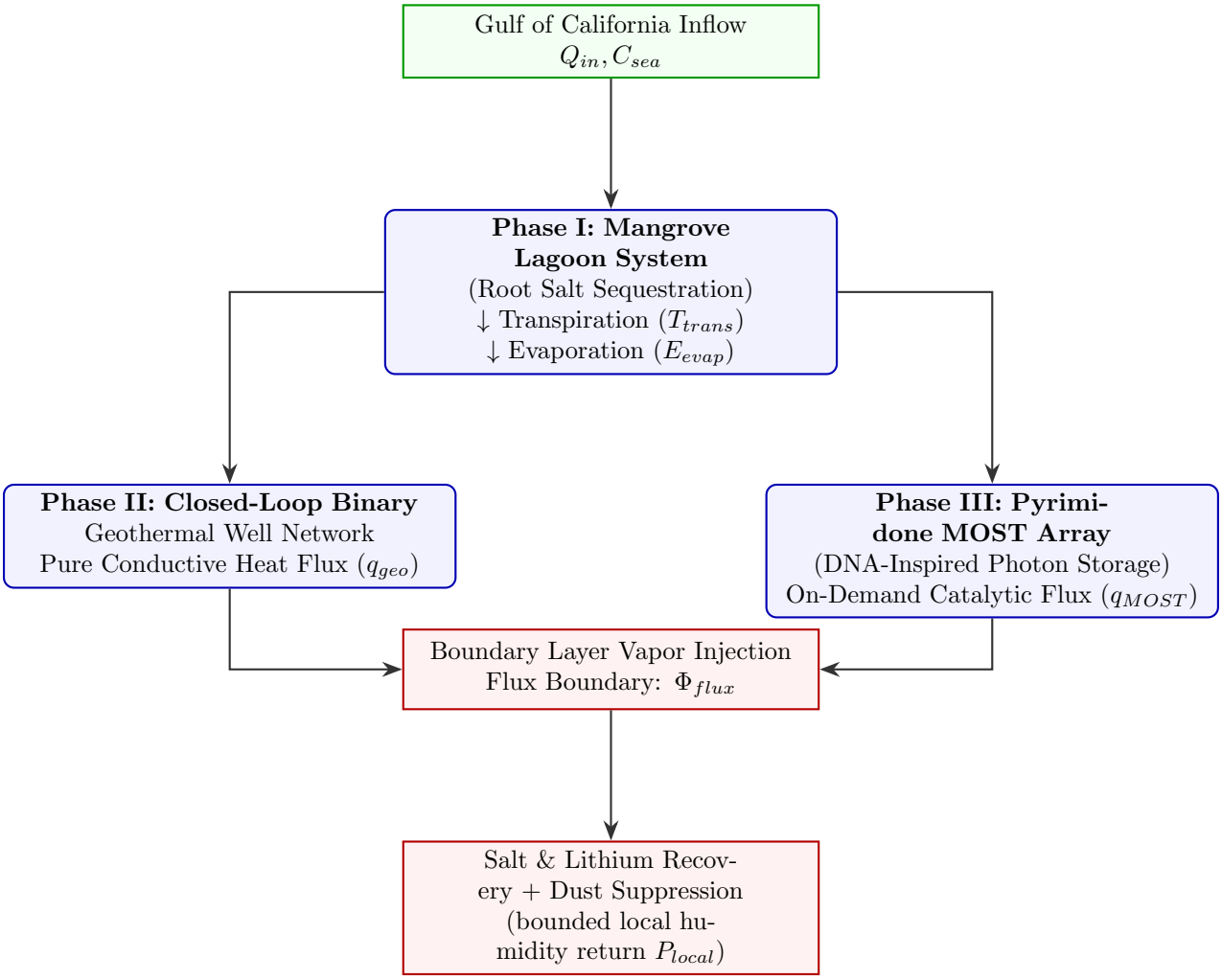

To demonstrate the physical viability of the BTVP (Biotic-Thermal Vapor Pump) framework, we establish the governing mass, salinity, thermodynamic, and atmospheric equations.

2.1 Mass and Salinity Balance in the Halophytic Basin

Let V represent the total liquid volume of the managed Laguna Salada basin (m^3), A_s represent the active surface area (m^2), Q_{in} represent the volumetric canal influx from the Gulf of California (m^3/s), and C represent the fluid salinity (kg/m^3). The timed mass balance of the liquid volume is governed by:

$$\frac{dV}{dt} = Q_{in} - A_s \left[E_{evap}(C, T_s) + T_{trans}(C, \kappa) \right]$$

Where E_{evap} is the direct physical evaporation rate (m/s), T_{trans} is the biological canopy transpiration rate (m/s), T_s is the surface water temperature (K), and κ is the leaf area index (LAI) of the mangrove forest.

The direct evaporation term must be modified to account for salinity-induced vapor pressure depression:

$$E_{evap}(C, T_s) = E_0 \cdot a_w(C) \cdot \left(\frac{e_s(T_s) - e_a}{e_s(T_s)} \right)$$

Where E_0 is the baseline evaporation rate of pure freshwater, $e_s(T_s)$ is the saturation vapor pressure at temperature T_s, e_a is the ambient vapor pressure, and $a_w(C)$ is the chemical activity of water, empirically modeled via a modified Raoult linear approximation for marine brines:

$$a_w(C) \approx 1 - \beta \left(\frac{C}{\rho_w} \right)$$

where $\beta \approx 0.537$ is the solute-effect constant and ρ_w is the density of pure water (1000 kg/m^3). The conservation of salt mass within the terminal basin floor is governed by:

$$\frac{d(V \cdot C)}{dt} = Q_{in} C_{sea} - S_{solid}(t)$$

Where $C_{sea} \approx 35$ kg/m^3 (35 ppt) is the source salinity of the Gulf of California, and $S_{solid}(t)$ is the mass extraction rate (kg/s) of dissolved solids removed as crystallized solid product. In contrast to unbuffered open evaporation—where $S_{solid} = 0$ and salt simply accumulates until a_w collapses—the BTVP routes a controlled fraction of the basin throughput across the laser-textured superwicking evaporator panels of Tang et al. [12]. There, the engineered groove geometry and coffee-ring advection continuously transport crystallizing NaCl, and the otherwise problematic Mg/Ca hard-scale phases, off the active evaporation region into passive collection zones, so that

$$S_{solid}(t) = \chi \cdot A_{panel} \cdot E_{panel} \cdot C \,,$$

where A_{panel} is the deployed panel area, E_{panel} is the panel-specific evaporation flux (m/s), and $\chi \leq 1$ is the solid-capture fraction (demonstrated near unity on Pacific, Atlantic, and Indian Ocean samples). A lithium-selective variant, achieved by embedding hydrogen-titanate nanoparticles in the panel grooves, additionally yields a recoverable lithium stream

$$\dot{m}_{Li}(t) = \phi_{Li} \cdot f_{Li} \cdot S_{solid}(t) \,,$$

with f_{Li} the lithium mass fraction of the incoming dissolved solids and $\phi_{Li} \approx 0.5$ the demonstrated lithium-recovery efficiency [13]. By maintaining a scale-asymmetric forest canopy, the transpiration term T_{trans} functions as a salt-buffered pump. Mangroves draw deep soil moisture upward and release it into the atmosphere, bound by an upper salinity threshold tolerance ($C_{max} \approx 90$ kg/m^3), above which $T_{trans} \to 0$. Thus, Q_{in} must be dynamically regulated to satisfy the steady-state boundary:

$$Q_{in} = A_s \left[E_{evap}(C) + T_{trans}(C) \right] \quad \text{at} \quad C \leq C_{max}$$

2.2 Thermodynamic Governing Equations (MOST and Geothermal Coupling)

To superheat the influx volume without risking the hydrovolcanic explosions or acid generation caused by pouring raw seawater directly onto magma, the total net thermal flux (q_{net}, W/m^2) delivered to the basin surface layer is partitioned as follows:

$$q_{net} = q_{solar} + q_{geo} + q_{MOST} - q_{sensible} - q_{latent} - q_{longwave}$$

The geothermal heat input (q_{geo}) is derived from closed binary loop deep wells that isolate the saline fluid from the magmatic basement:

$$q_{geo} = \frac{N_{wells} \cdot \dot{m}_{cf} \cdot C_p \cdot (T_{outflow} - T_{inflow})}{A_s}$$

Where N_{wells} is the number of operating borehole heat exchangers, $\dot{m}_{cf}$ is the mass flow rate of the demineralized working fluid (kg/s), C_p is its specific heat capacity, and $T_{outflow}$ is restricted by the safe convective

thermal limits of the Laguna Salada reservoir ($T_{max} \approx 187°C = 460.15$ K). This completely suppresses the phreatomagmatic eruption pathway ($P_{steam} < P_{lithostatic}$) and avoids HCl outgassing. The on-demand Molecular Solar Thermal flux (q_{MOST}) utilizes the pyrimidone structural isomer reversion mechanics discovered in 2026. Sunlight strikes the configured pyrimidone molecular arrays, causing a reversible photoisomerization that stores energy in chemical bonds for extended durations without thermal leakage:

$$\text{Pyrimidone (State A)} + h\nu \xrightarrow{\eta} \text{Photoisomer (State B)}$$

Upon introduction of a localized solid-phase catalyst surface, State B rapidly reverts to State A, releasing stored enthalpy (ΔH_{MOST}, J/mol) as pure sensible heat:

$$q_{MOST}(t) = \delta(t - t_{active}) \cdot \frac{\gamma \cdot M_{poly} \cdot \Delta H_{MOST}}{A_s}$$

Where δ is the Dirac delta modulation function representing catalytic activation at the optimal meteorological window t_{active}, γ is the conversion efficiency of the catalyst interface, and M_{poly} is the total moles of active pyrimidone material deployed within the feeder channels.

2.3 Atmospheric Boundary Layer Coupling and Bounded Moisture Return

The total mass flux of water vapor injected into the local atmospheric boundary layer (Φ_{flux}, kg/s) is determined by the combined latent heat terms:

$$\Phi_{flux} = \frac{A_s \cdot (q_{latent,evap} + q_{latent,trans})}{L_v}$$

Where L_v is the latent heat of vaporization ($\approx 2.26 \times 10^6$ J/kg). For the managed footprint considered here this corresponds to a gross injection of order $\Phi_{flux} \sim 3.8 \times 10^8\,\mathrm{m^3/yr}$ (Section 4.1).

It is essential to characterize honestly what fraction of this injection can return as precipitation within the Salton Sea watershed, because earlier "pump-and-rain" framings have over-attributed basin recharge to this pathway. Two independent bounds apply.

First, a *moisture-budget bound*. The vertically integrated vapor transport (IVT) through the region under non-atmospheric-river conditions is of order 100–250 $\mathrm{kg\,m^{-1}s^{-1}}$. Across a crosswind source width of $w \approx \sqrt{200\,\mathrm{km}^2} \approx 14\,\mathrm{km}$, the natural moisture flux traversing the source corridor is $Q_{atm} = \mathrm{IVT} \cdot w \approx 4$–$11 \times 10^{10}\,\mathrm{m^3/yr}$ (water-equivalent). The injected flux is therefore only

$$\frac{\Phi_{flux}}{Q_{atm}} \approx 0.3\text{–}0.9\%$$

of the moisture already advecting through the airspace. A perturbation at the sub-percent level cannot be deterministically steered onto a chosen orographic barrier; it is entrained into, and largely transported by, the prevailing synoptic flow.

Second, a *precipitation-recycling bound*. The fraction of locally evaporated water that precipitates within the same region (the recycling ratio ρ_{rec}) is, in standard bulk formulations [20, 21], approximately

$$\rho_{rec} \approx \frac{E\,L}{E\,L + 2\,Q'_{atm}}\,,$$

where E is the areal evaporation rate, L the along-flow length scale of the source, and Q'_{atm} the per-unit-width moisture flux. For source length scales of 15–100 km and the IVT values above, $\rho_{rec} \approx 0.3$–2%. The in-region precipitation attributable to the injection is therefore bounded at

$$P_{local} = \rho_{rec}\,\Phi_{flux} \approx 1\text{–}7 \times 10^6\,\mathrm{m^3/yr},$$

one to two orders of magnitude below the volumes assumed by prior open-evaporation concepts, and small relative to the Salton Sea's net deficit ($\sim 10^9\,\mathrm{m^3/yr}$). We therefore do *not* claim that the BTVP refills the Salton Sea by engineered precipitation. The MOST timing actuator (Section 2.2) can bias the modest recycled fraction toward favorable wind windows ($\cos\theta_{wind} \to 1$, low LCL), improving the *efficiency* of whatever return occurs, but cannot lift it past the budget ceiling set above. The defensible atmospheric benefit is local humidity and microclimate modification over the managed basin—which suppresses dust mobilization and moderates surface temperature—rather than downwind basin recharge.

3 Discussion

The Biotic-Thermal Vapor Pump represents a convergence of three independently validated scientific domains — halophytic ecology, closed-loop geothermal engineering, and photochemical molecular storage — into a single coherent geoengineering architecture. This section examines each subsystem in greater mechanistic depth, introduces visual frameworks for each phase, and contextualizes the integrated design against the broader literature on precipitation enhancement and transboundary water management.

3.1 Phase I - Halophytic Canopy as a Controlled Vapor Pump

The selection of *Avicennia germinans* and *Rhizophora mangle* as the primary silvicultural agents is grounded in their documented physiological tolerance under extreme arid, high-salinity conditions. Research on *Avicennia marina* populations in the Arabian Gulf demonstrates survival at pore-water salinities of 50–60 PSU under hyper-arid conditions, far exceeding typical seawater concentrations of 35 PSU, due to leaf-level salt-secreting glands and xeromorphic leaf architecture that simultaneously limit excessive transpiration while maintaining viable moisture uplift [16]. Critically for the BTVP (Biotic-Thermal Vapor Pump) design, mangroves in arid climates form short, dense forests dominated by *Avicennia* species, and their primary existential threat is precisely the hydrological modification that causes hypersalinity — the same boundary condition the BTVP is engineered to maintain below the $C_{max} \approx 90\,\mathrm{kg/m^3}$ tolerance ceiling [6]. The transpiration pathway is fundamentally distinct from mechanical evaporation. Where open-surface evaporation is directly suppressed by rising salinity via Raoult's Law (see Eq. 2), the biological salt-exclusion mechanisms at the mangrove root zone decouple the atmospheric moisture flux from bulk basin salinity within the operational range $C \leq C_{max}$. The root ultrafiltration acts as a living reverse-osmosis membrane, enabling continuous low-salinity vapor release even as the basin brine concentration rises. This bistable hydro-ecological feedback — where the mangrove canopy itself moderates the salinity gradient through regulated transpiration — has been formally demonstrated in mathematical models of halophytic versus freshwater community competition [5]. Figure 1 illustrates the multi-layer moisture pathway from basin surface through the mangrove root-stem-leaf system to the atmospheric boundary layer.

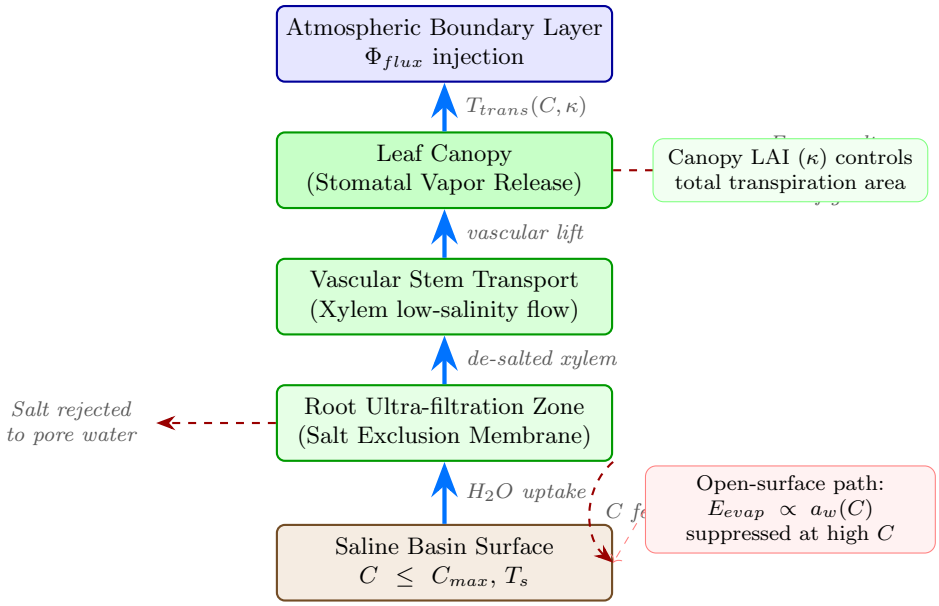

Figure 1: Phase I moisture pathway. Saline basin water is drawn upward through the mangrove root ultrafiltration membrane, which decouples transpiration flux from bulk brine salinity. Salt is rejected laterally into the pore water and expelled via leaf glands, while low-salinity water vapor is released at the canopy into the atmospheric boundary layer. This biological pathway circumvents the Raoult's Law suppression that shuts down open-surface evaporation at high C.

3.2 Phase I (engineered) - Brine-Free Solar-Thermal Evaporation and Mineral Recovery

The biotic canopy of the preceding section solves moisture uplift but cannot, by itself, close the terminal-basin salt budget: salt rejected at the root zone still accumulates in the bulk brine. The 2026 University of Rochester solar-thermal desalination architecture [12] supplies precisely the missing sink. Laser-textured superwicking black metal absorbs nearly all incident sunlight and draws a thin film of basin water across an active region; as the film evaporates, microscopic groove patterning and the coffee-ring effect advect crystallizing salts—including the dense Mg/Ca scale phases that clog conventional interfacial evaporators—toward passive collection zones, yielding continuous, self-cleaning operation and recovering nearly all dissolved solids in solid form rather than as discharged brine. The companion study [13] demonstrates that embedding hydrogen-titanate nanoparticles in the same grooves selectively isolates lithium, with $\approx 50\%$ recovery from Great Salt Lake water. Within the BTVP this converts the basin's principal failure mode—hypersaline shutdown and a secondary toxic playa in Mexico—into a managed, revenue-bearing mineral stream.

Energy-budget scalability (solar physics). Because the process is solar-thermal, its output is capped by the available insolation, not by the device. For the Laguna Salada / Imperial Valley region (24-hour-average global horizontal irradiance $G \approx 271\,\mathrm{W/m^2}$, among the highest in North America), the depth-equivalent evaporation rate is $E = \eta\, G/(L_v\, \rho_w)$. At solar-to-vapor efficiencies of $\eta = 0.50$–0.85 this yields 1.9–3.2 m/yr per square metre of active surface (Table 1). To supply the framework's target injection of $\Phi_{flux} \approx 3.8 \times 10^8\,\mathrm{m^3/yr}$ therefore requires roughly 120–200 $\mathrm{km^2}$ of active evaporator—consistent with the assumed 200 $\mathrm{km^2}$ managed footprint. The area-scale physics is thus internally coherent.

It must be stated plainly, however, that the engineered evaporator does *not* increase the vapor ceiling: a bare 200 $\mathrm{km^2}$ open basin at the local pan-evaporation rate (≈ 1.8 m/yr) already evaporates $\approx 3.6 \times 10^8\,\mathrm{m^3/yr}$. The strategic contribution of the Rochester architecture is therefore *not* additional moisture flux but (i) elimination of the brine/scaling shutdown that caps the *sustainable* fraction of that evaporation, and (ii) recovery of salts and lithium as solid co-products. This reframing strengthens rather than weakens the case: the technology resolves the exact failure mode (Eq. 2, $a_w(C)$ collapse) identified for unbuffered schemes in the Introduction.

Manufacturing scalability (the binding constraint). The honest limiting question is not the physics but the fabrication throughput of femtosecond-laser surface texturing at $\mathcal{O}(100)\,\mathrm{km^2}$ scale. Reported fs-laser blackening/wicking throughputs span $\sim$ 1–10 $\mathrm{cm^2/s}$ per station for research systems, rising toward $\sim$ 100–1000 $\mathrm{cm^2/s}$ only with high-power industrial polygon-scanner architectures. Texturing 200 $\mathrm{km^2}$ within a two-year build window correspondingly demands the laser-station fleets summarised in Table 1: of order 10^4 stations at present research rates, falling to a plausible ~ 30 stations only at the most optimistic industrial throughput. Full-footprint deployment is therefore *not* demonstrably scalable on current throughput, and we do not claim otherwise; the realistic near-term pathway is a hybrid in which the engineered panels line only the high-evaporation feeder channels and salt-management cells (a few percent of the footprint), with the open biotic basin carrying the bulk of the area. Advancing roll-to-roll or high-repetition-rate laser texturing is the single most important enabling research direction for the engineered layer, and we flag it explicitly as an open problem rather than a solved one.

Table 1: Scalability summary for the engineered solar-thermal evaporation layer. Solar physics is consistent with the 200 $\mathrm{km^2}$ footprint; femtosecond-laser fabrication throughput is the binding constraint.

Quantity	**Value / range**	**Basis**
Evaporation rate (per $\mathrm{m^2}$)	1.9–3.2 m/yr	$\eta = 0.50$–0.85, $G = 271\ \mathrm{W/m^2}$
Active area for $3.8 \times 10^8\ \mathrm{m^3/yr}$	120–200 $\mathrm{km^2}$	solar energy budget
Open-basin baseline (200 $\mathrm{km^2}$)	$3.6 \times 10^8\ \mathrm{m^3/yr}$	pan evap ≈ 1.8 m/yr
fs-laser fleet to texture 200 $\mathrm{km^2}$ in 2 yr	$\sim 3 \times 10^4$ stations	at 1 $\mathrm{cm^2/s}$/station
	$\sim$30 stations	at 1000 $\mathrm{cm^2/s}$/station
Lithium from Gulf inflow ($Q_{in} = 5\ \mathrm{m^3/s}$)	≈ 13 t/yr	0.17 mg/L Li, 50% recovery

Lithium co-product in context. At open-ocean lithium concentration ($\approx 0.17\,\mathrm{mg/L}$) the recoverable lithium from a $5\,\mathrm{m}^3/\mathrm{s}$ canal inflow is only $\approx 13\,\mathrm{t/yr}$—a useful offset against operating cost but small against a mid-size hard-rock mine (10,000–20,000 t/yr). The economically decisive lithium resource in this region is not the Gulf inflow but the Salton Sea geothermal brine itself, which carries $\sim$ 100–300 mg/L lithium—roughly three orders of magnitude richer. The Phase II closed-loop network therefore offers a natural, far higher-grade feedstock for the same hydrogen-titanate selective-recovery chemistry, coupling the BTVP directly to the emerging "Lithium Valley" resource without requiring open contact with the corrosive native brine.

3.3 Phase II - Closed-Loop Geothermal Architecture

The deep borehole heat exchanger (DBHE) configuration selected for the BTVP is a coaxial closed-loop design in which a dedicated working fluid — demineralized water or a high-boiling binary organic compound — circulates entirely within a sealed annular downhole loop. This arrangement is critical because it achieves conductive heat exchange with the 187°C Laguna Salada geothermal reservoir without any hydraulic contact between the working fluid and the native saline formation water. Peer-reviewed DBHE modeling studies confirm that closed-loop systems can achieve energy production-to-investment ratios of approximately 7 GJ/GJ [7], and sensitivity analyses on volcanic settings analogous to the Laguna Salada sub-basin show achievable energy flow rates of up to 1.5 MW per well with optimized annulus geometry [17].

The safety advantage over open-loop injection is thermodynamically absolute: by restricting the working fluid within the sealed loop, steam pressure at the wellhead is governed by the controlled pump circulation rate rather than by the uncontrolled flash evaporation of injected seawater. This enforces the condition $P_{steam} < P_{lithostatic}$ at all operating points, eliminating the phreatomagmatic eruption pathway documented by Mattox and Mangan [18]. Similarly, because the native formation fluid never contacts the surface heat exchangers, halite hydrolysis and HCl outgassing is thermodynamically impossible within the BTVP (Biotic-Thermal Vapor Pump) architecture.

Figure 2 shows the coaxial downhole heat exchanger configuration and the surface binary-cycle coupling to the basin heat distribution network.

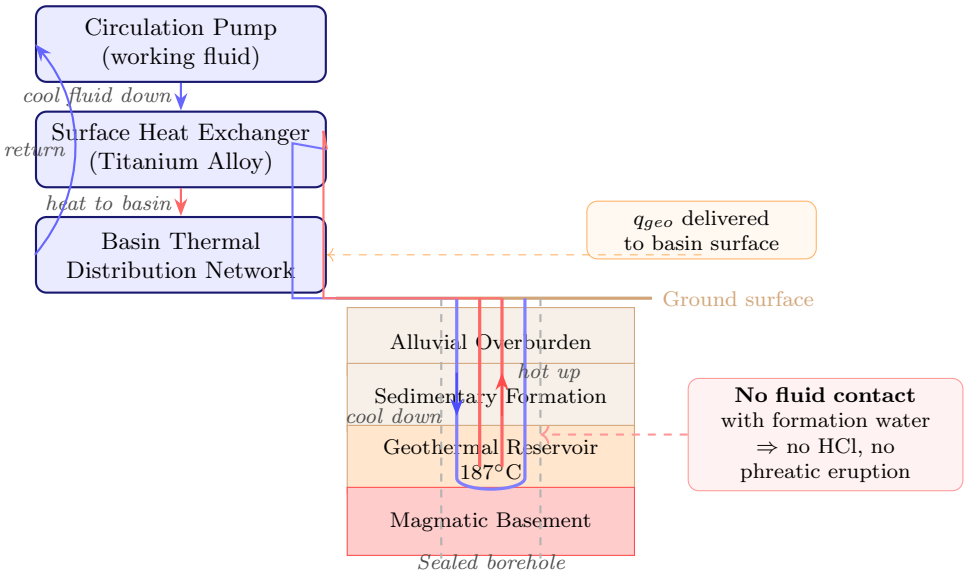

Figure 2: Phase II closed-loop coaxial borehole heat exchanger (DBHE) schematic. Cool working fluid descends in the outer annulus, absorbs conductive heat from the 187°C reservoir, and returns to the surface in the inner pipe. Sealed loop geometry prevents any hydraulic contact between the working fluid and native saline formation fluids, eliminating both phreatomagmatic and HCl hazard pathways.

3.4 Phase III - Temporal Scheduling via MOST Photochemistry

The 2026 publication by Nguyen, Han, Houk, and collaborators in *Science* established the first pyrimidone-based MOST (Molecular Solar Thermal) system to simultaneously exceed the practical benchmarks of energy storage density ($> 1.6\,\mathrm{MJ/kg}$), multi-year ambient-temperature stability, aqueous compatibility, and controllable acid-triggered heat release [11]. The molecule operates in a solvent-free Dewar photoisomer state after UV excitation at 300 nm, and delivers rapid heat release upon introduction of a solid-phase acid catalyst — precisely the controllable "trigger" mechanism exploited by the BTVP Phase III architecture. Notably, the design philosophy explicitly prioritized compactness and recyclability: the protonated pyrimidone is neutralized after heat release and recharged by re-exposure to sunlight, making the MOST array a renewable, on-demand thermal battery rather than a consumable reagent [8].

The strategic value of Phase III within the BTVP is not raw thermal power — the geothermal BHE array provides the bulk baseline heating — but rather *temporal precision*. By storing solar energy during the day and releasing it only when synoptic wind analysis confirms that $\cos(\theta_{wind}) \to 1$ (favorable south-to-north transport toward the California mountain ranges) and the lifting condensation level is anomalously low, the MOST array functions as a meteorological actuator. This concept parallels the emerging class of "smart cloud seeding" programs identified in the UAE Rain Enhancement Program, which integrate machine-learning wind targeting and autonomous seeding systems to maximize orographic yield per unit of moisture injected [19].

Figure 3 shows the photochemical charging and catalytic discharge cycle as integrated within the BTVP feeder channels.

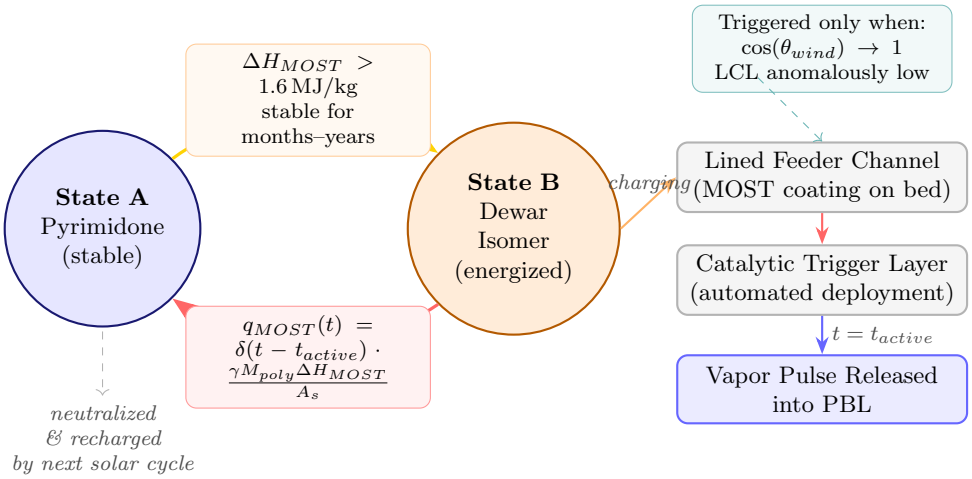

Figure 3: Phase III MOST photochemical cycle. Pyrimidone molecules are photocharged from State A to the strained Dewar isomer (State B) by ambient UV. Stored energy ($> 1.6\,\mathrm{MJ/kg}$) remains stable for months until an automated acid catalyst is deployed at the meteorological trigger window t_{active}, releasing a precise pulse of sensible heat into the feeder channel water and driving a timed Φ_{flux} spike into the planetary boundary layer.

3.5 Integrated System Dynamics

The three phases operate in a coupled hierarchy: Phase I provides the continuous baseline moisture flux T_{trans} and the brine-free salt/mineral sink; Phase II elevates surface water temperature to amplify E_{evap}, reduces salinity stratification, and supplies high-grade lithium feedstock; Phase III modulates the total flux Φ_{flux} with event-scale precision. It is important to state the limit of this coordination precisely. The MOST timing actuator can bias the *timing* of vapor release toward windows of low convective inhibition and favorable wind alignment ($\cos\theta_{wind} \to 1$), improving the efficiency of whatever moisture return occurs; it cannot, however, raise that return past the moisture-budget and recycling-ratio ceilings established in Section 2.3. We are therefore explicit that the system does not convert a sub-percent local moisture perturbation into a

"deterministic precipitation signal" over the watershed—a claim the physics does not support—and we have removed that framing accordingly. What the integrated architecture *does* deliver is a self-consistent, hazard-bounded remediation engine: imported Gulf water is evaporated under managed conditions that recover its salt and lithium content as solid product (eliminating the brine-discharge obstacle that ended prior Sea-to-Sea review [2]), the playa surface is stabilized and revegetated to suppress toxic dust, and local humidity is modestly elevated. The fundamental dynamics of orographic precipitation—moist instabilities, blocking flows, and windward-slope convective initiation—remain well characterized in the literature [20, 21], and the broader Clausius–Clapeyron scaling of precipitable water with temperature [15] applies to the synoptic environment; neither, however, licenses attributing watershed-scale recharge to a 14 km engineered source. Figure 4 presents a unified energy and moisture flow diagram spanning all three phases and the downstream atmospheric pathway.

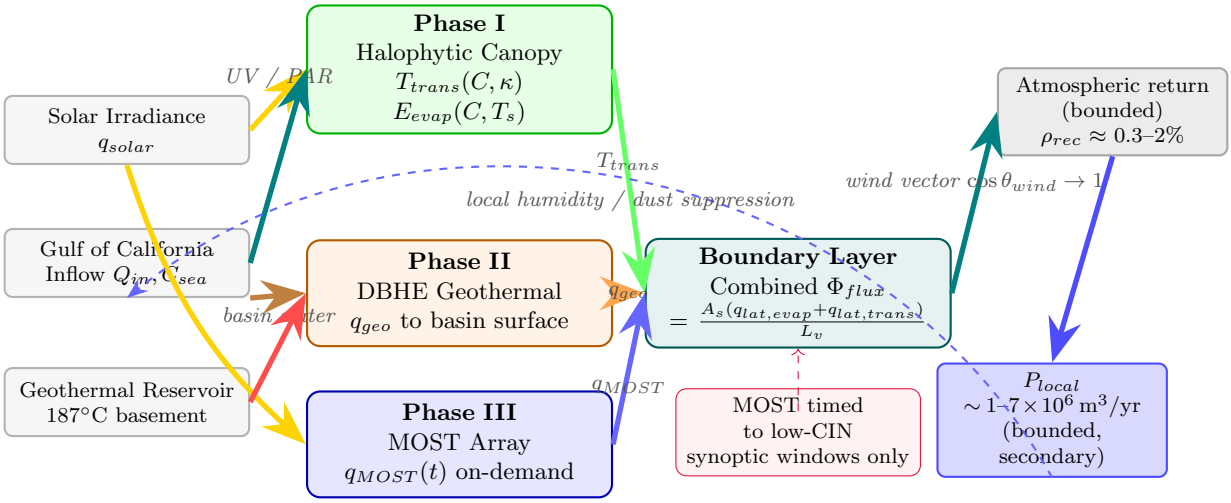

Figure 4: Integrated BTVP energy and moisture flow diagram. Solar irradiance simultaneously charges the Phase I canopy (via photosynthetically active radiation driving transpiration) and the Phase III MOST array (via UV photoisomerization). Gulf of California inflow provides the water mass budget. Geothermal heat from the closed-loop DBHE (deep borehole heat exchanger) network elevates basin surface temperature. All three thermal and moisture terms combine at the atmospheric boundary layer into Φ_{flux}, which is scheduled for orographic transport only during optimal synoptic windows. Net downwind precipitation recharges the Salton Sea basin, closing the hydrological loop.

3.6 Comparative Assessment and Novel Insights

Salinity self-regulation as an emergent system property. A key emergent feature of the BTVP that warrants explicit discussion is the negative-feedback salinity control arising from the interplay of Phases I and II. As basin salinity C rises toward C_{max}, Phase I transpiration $T_{trans} \to 0$, reducing the net evaporative draw on Q_{in}. This reduction accumulates a dilution reserve that, combined with the thermal stratification imposed by Phase II, drives convective mixing and saline front suppression. The result is a self-regulating brine concentration that asymptotically approaches — but does not reach — the mangrove tolerance ceiling, without requiring active chemical intervention.

MOST energy density in the geoengineering context. The pyrimidone Dewar isomer system stores > 1.6 MJ/kg, a value that compares favorably with standard lithium-ion batteries (≈ 0.5–0.9 MJ/kg usable thermal equivalent) [9]. For a 200 km^2 active BTVP footprint, even a thin 1 mm coating of pyrimidone at a conservative areal density yields a stored energy reserve sufficient for multiple high-intensity vapor release events per week without intermediate recharging — particularly advantageous given the Laguna Salada region's near-constant high-UV solar irradiance.

Transboundary governance as a design constraint. The BTVP is explicitly transboundary: the evaporation and mineral-recovery infrastructure sits in Baja California, Mexico, while much of the public-health benefit and the institutional impetus originate in California, USA. A gulf-sourced route also requires a new bilateral water treaty, a constraint identified in every serious Sea-to-Sea assessment [2, 1]. This governance layer must be treated as an engineering constraint equivalent in importance to the thermodynamic specifications, and benefit-sharing is more tractable when the shared product is tangible and divisible—desalinated water, recovered salts, and lithium—rather than a diffuse and uncertain downwind precipitation claim. Recovered-mineral revenue, in particular, provides a concrete basis for binational cost- and benefit-sharing agreements.

Relationship to cloud seeding. It is worth distinguishing the BTVP from conventional cloud seeding [22, 19], since both are sometimes grouped as "precipitation enhancement." Cloud seeding injects condensation nuclei into pre-existing clouds to improve in-cloud precipitation efficiency. The BTVP is not a precipitation-enhancement technology in this sense: as Section 2.3 shows, its moisture injection is a sub-percent perturbation on the synoptic budget and cannot manufacture a precipitating cloud field where none would otherwise form. We therefore make no precipitation-enhancement claim. The BTVP's atmospheric footprint is confined to local humidity and microclimate effects over the managed basin; its principal value lies in remediation and resource recovery, not weather modification.

4 Stage 1 Implementation: Costs, Timeline, and Projected Outcomes

4.1 Projected Outcomes

Assuming an active managed footprint of $200\,\mathrm{km}^2$ within the Laguna Salada basin, the framework's projected outcomes, each bounded against the governing physics, are:

- **Gross atmospheric moisture injection (Φ_{flux}):** combined baseline evaporation, closed-loop thermal enhancement, and canopy transpiration lift of order $3.8 \times 10^8\,\mathrm{m}^3$ of water vapor into the boundary layer annually. As shown by the energy-budget analysis (Table 1), this is solar-capped and comparable to what an equivalent open surface would evaporate; the engineered layer's value is brine-free salt handling, not additional flux.
- **Local atmospheric return (P_{local}):** bounded by moisture-budget and recycling-ratio analysis (Section 2.3) at $\sim$ 1–$7 \times 10^6\,\mathrm{m}^3/\mathrm{yr}$ within the region—one to two orders of magnitude below earlier "pump-and-rain" projections and small against the basin deficit. We present this as a secondary humidity/microclimate and dust-suppression benefit, not as basin recharge.
- **Salt and mineral recovery:** near-complete capture of imported dissolved solids in solid form, eliminating brine discharge—the decisive obstacle in prior review [2]—and yielding a saleable salt stream.
- **Lithium co-product:** of order $10\,\mathrm{t/yr}$ from the Gulf inflow at seawater concentration, rising substantially if the lithium-selective recovery chemistry is applied to the Phase II geothermal brine ($\sim$ 100–$300\,\mathrm{mg/L}$), coupling the project to the regional "Lithium Valley" resource.
- **Dust and public-health benefit:** stabilization and revegetation of the managed surface to suppress wind-driven mobilization of arsenic- and pesticide-laden particulates.

The primary, defensible case for the BTVP rests on the last three items; the first two are reported with explicit physical bounds rather than as headline water-supply claims.

4.2 Capital Cost Estimates

The implementation of the BTVP requires capital allocation across infrastructure, hydrogeology, and advanced chemical manufacturing sectors:

Project Element	Description	Estimated Cost (USD)
Conveyance Infrastructure	Dredging, widening 40 miles of Coyote Canal; excavating 25 miles of sea-level gravity channels. No high-lift pumping stations required.	$105,000,000
Phase I Silviculture	Black and Red Mangrove cultivation, soil stabilization, engineered sub-cell embankments, and initial nutrient seeding.	$45,000,000
Phase II Geothermal	Installation of 18 closed-loop binary downhole borehole heat exchangers (BHE) tapping the 187°C reservoir, including titanium alloy top-side heat exchangers.	$135,000,000
Phase III MOST Array	Industrial synthesis of modified pyrimidone matrices, application to shallow lined feeder channels, and automated catalytic trigger deployment.	$110,000,000
Contingency and Oversight	Transboundary environmental monitoring, legal/treaty frameworks, and unexpected geographic adjustments.	$65,000,000
TOTAL ESTIMATED CAPEX		$460,000,000

The figures above assume the engineered solar-thermal evaporator is deployed selectively along feeder channels and salt-management cells rather than across the full footprint. Full-footprint femtosecond-laser texturing would raise capital cost by one to two orders of magnitude at present fabrication throughput (Table 1); the cost of the engineered layer is therefore governed almost entirely by laser-texturing throughput and constitutes the dominant cost uncertainty in the entire framework. This is treated as an explicit research-gap risk rather than a fixed line item.

4.3 Execution Timeline

The project is structured across a multi-stage rollout to allow natural biological stabilizing mechanisms to mature before maximizing thermal vapor forcing:

- Year 1-2: Phase I - Canal Excavation and Halophytic Colonization: 1. Canal dredging and gravity-inflow initiation. 2. Mangrove cultivation and root matrix establishment
- Year 3-4: Phase II - Closed-Loop Geothermal Integration: 1. Deep directional well drilling (BHE loops) 2. Benthic titanium heat exchanger installation
- Year 5-7: Phase III - Advanced MOST Material Optimization: 1. Pyrimidone channel coating and catalyst installation. 2. Full synchronization of on-demand orographic vapor cycles

Through this phased development, the project transitions from a heavily monitored engineering footprint into a self-sustaining, microclimatic driver. The BTVP serves as a landmark model for transboundary ecological engineering, proving that advanced thermodynamic materials and nature-based solutions can cooperate to remediate severe regional environmental crises.

4.4 Transient Hydro-Geochemical Trajectories and the Hydrological Deficit Wall

To map the long-term remediation velocity of the basin under active hybrid extraction, we implement a dynamic, forward-integrating box model tracking the temporal evolution of lake volume $V(t)$, total dissolved salt mass $S(t)$, and bulk salinity $C(t) = S(t)/V(t)$. The system is governed by coupled ordinary differential equations mapping localized bathymetric variations, natural evaporation surfaces, agricultural tailwater returns, and targeted desalination intake layouts:

$$\frac{dV}{dt} = Q_{\text{in}} - E_{\text{nat}} A(V) - Q_{\text{plant}}(t)(1 - Y_{\text{ro}}) \tag{1}$$

$$\frac{dS}{dt} = Q_{\text{in}} C_{\text{in}} - Q_{\text{plant}}(t) C(t) \eta_{\text{rejection}} \tag{2}$$

where $Q_{\text{in}} = 1.05\,\text{km}^3/\text{yr}$ represents projected future agricultural inflows, $C_{\text{in}} = 2.8\,\text{g/L}$ is the incoming runoff salinity baseline, $E_{\text{nat}} = 1.78 \times 10^{-3}\,\text{km/yr}$ is the hyper-arid evaporation rate, and $A(V)$ is an empirical power-law fit derived from basin bathymetry ($A(V) = 900(V/7.5)^{0.68}$).

A critical, non-intuitive architectural boundary emerges when analyzing this dynamic system: the terminal basin's structural water deficit wall. At the initial target ecological volume of $4.5\,\text{km}^3$, the localized surface area spreads to $\sim 635\,\text{km}^2$, generating an atmospheric evaporative loss of $\sim 1.13\,\text{km}^3/\text{yr}$. Because this natural evaporative output inherently exceeds the stable agricultural inflow ($1.05\,\text{km}^3/\text{yr}$), the basin possesses a baseline negative water balance independent of any technological intervention.

Consequently, a naive control architecture designed to prioritize volume preservation by shutting down plant operations ($Q_{\text{plant}} \to 0$) when $V(t) \leq 4.5\,\text{km}^3$ triggers an ecological failure mode. While the water volume temporarily stabilizes near the bathymetric floor, the unceasing agricultural influx deposits 2.94×10^6 metric tonnes of salt annually into the terminal sink. Without active processing, the salinity bounds upward continuously, exceeding 99.3 g/L within a 40-year window, rendering the lake ecologically dead.

To circumvent this boundary, the hybrid system must employ a *Salt-Mass Balance Priority* control loop. When the basin reaches the target ecological floor, the system throttles the high-throughput SWRO facility from its maximum accelerated remediation capacity ($1.25\,\text{km}^3/\text{yr}$) down to a steady-state maintenance flux calculated directly from the real-time mass balance:

$$Q_{\text{plant, ss}} = \frac{Q_{\text{in}} C_{\text{in}}}{C_{\text{target}} \eta_{\text{rejection}}} \tag{3}$$

Setting $C_{\text{target}} = 35.0\,\text{g/L}$ (marine equivalence) requires a permanent maintenance throughput of $Q_{\text{plant, ss}} \approx 0.085\,\text{km}^3/\text{yr}$. This active mass extraction forces the basin into a final, physically locked equilibrium at $V_{\text{ss}} \approx 3.75\,\text{km}^3$ and $C_{\text{ss}} = 35.0\,\text{g/L}$. The BTVP framework acts as the permanent mineral sink for this loop, crystallizing exactly 2.94 M t/yr of solid crystalline co-products, satisfying both water-balance constraints and long-term salinity stabilization rules.

5 Stage 2: Direct Salton Sea Restoration via Brine-Free Importation and Geothermal Lithium Co-Production

The framework developed above remediates the Laguna Salada basin and proves the brine-free desalination and zero-liquid-discharge (ZLD) mineral-mining chain at field scale. It does not, by itself, refill the Salton Sea—the moisture-budget analysis of Section 2.3 forecloses that pathway. We therefore frame the present design as **Stage 1** of a two-stage program: a self-justifying remediation and resource-recovery installation on the Mexican side that simultaneously de-risks the technology required for **Stage 2**, direct stabilization of the Salton Sea itself.

The strategic significance of Stage 1 is that it dissolves the single decisive *environmental* objection of the 2022 Independent Review Panel [2]. Of the three obstacles the Panel raised against direct Gulf importation—cost, timeline, and brine discharge—the brine-discharge harm to the Gulf of California was the one with no prior engineering answer. The Rochester additive-free, brine-discharge-free architecture [12, 13] provides exactly that answer: the desalination concentrate that earlier schemes would have returned to the Sea of Cortez is instead crystallized to solids and mined for lithium. Stage 2 thus becomes a conventional water-conveyance problem coupled to a ZLD backend, rather than a marine-pollution problem.

What Stage 2 cannot be, and what it must be. Solar-thermal distillation alone cannot supply bulk restoration water. To offset the Salton Sea's net deficit ($\sim 8 \times 10^8\,\text{m}^3/\text{yr}$) by solar evaporation at $\approx 2.8\,\text{m/yr}$ would require $\approx 290\,\text{km}^2$ of laser-textured panel; matching the historical Sea-to-Sea import figure (2.8 million acre-feet/yr, $\approx 3.5 \times 10^9\,\text{m}^3/\text{yr}$) would require $\approx 1{,}200\,\text{km}^2$—squarely against the femtosecond-laser manufacturing wall identified in Section 3.2. The realistic Stage 2 architecture is therefore a *hybrid*: established high-throughput desalination (reverse osmosis or thermal) produces the bulk freshwater conveyed north, while the brine-free solar-thermal stage serves as the ZLD concentrate processor that eliminates the

brine stream and recovers minerals. The role of the Rochester technology is not to make all the water; it is to make the project environmentally admissible and partially self-financing.

5.1 Treatability Constraints and Hybridization with Membrane Desalination

The practical realization of Stage 2 requires addressing the extreme geochemical and organic impairments of the modern Salton Sea, which has transitioned into a hyper-eutrophic, hypersaline sink. Pontius [30] evaluated the direct treatability of Salton Sea surface water (salinity $\sim$ 43 ppt, total dissolved solids $\sim$ 70,000 mg/L, and a severe apparent color constraint of 1440 CU), demonstrating the fundamental limitations of standard municipal treatment loops. Conventional coagulation-sedimentation using aluminum chlorohydrate, ferric chloride, or alum proved highly ineffective for turbidity removal, with alum achieving a maximum color removal efficiency of only 28% at a high dose of 40 mg/L [30]. However, Pontius established that multi-stage membrane separation—utilizing 0.1 μm to 0.45 μm microfiltration followed by Seawater Reverse Osmosis (SWRO)—successfully achieves exceptional initial contaminant rejections: 99% for bulk salinity, 98.6% for TDS, and 99.3% for turbidity [30].

While the Pontius model confirms that high-rejection SWRO is technically viable for processing Salton Sea water for environmental stabilization or potential urban diversion, its deployment as a standalone framework introduces a severe secondary crisis: the generation of vast volumes of hyper-concentrated, toxic brine. In a closed terminal basin, discharging this membrane concentrate back into the lake bed would catastrophically accelerate salinity scaling and ecological collapse, while terrestrial evaporation ponds require prohibitive land footprints.

The BTVP framework directly extends the Pontius model by providing the missing Zero-Liquid-Discharge (ZLD) coupling. Rather than relying on solar-thermal surfaces to process the raw water deficit outright—which hits the laser manufacturing throughput wall identified in Section 3.2—the optimal Stage 2 architecture utilizes a symbiotic hybrid loop. High-throughput SWRO facilities, configured using the microfiltration pre-treatment parameters validated by Pontius [30], generate the bulk freshwater volume. The resulting hyper-impaired brine concentrate stream is then routed directly to the BTVP's laser-textured superwicking solar evaporators and halophytic canopy. By utilizing the coffee-ring crystallization and biological root-zone ultrafiltration described in Section 3, the BTVP serves as a specialized solid-phase processor that crystallizes the SWRO waste stream into stable, solid mineral co-products. This symbiosis resolves the primary environmental and disposal bottlenecks of conventional membrane desalination in impaired terminal basins, transforming a toxic waste liability into a financeable mineral-extraction engine.

Stage 2 mass, energy, and materials budget. Table 2 summarizes a first-order budget for the deficit-offset target. The headline result is favorable for the environmental case and sobering for the logistics: routing the concentrate through ZLD eliminates $\sim 10^9\,\mathrm{m}^3$/yr of marine brine discharge, but converts it into $\sim$ 60 Mt/yr of solid salts—a mass that vastly exceeds any salt market and constitutes a major solid-handling and beneficial-use challenge in its own right (gypsum, magnesia, and halite byproducts; engineered fill; sequestration). The lithium co-product at Gulf-seawater grade is modest ($\sim$ 150 t/yr) but rises by up to three orders of magnitude in concentration if the same selective chemistry is applied to the Phase II geothermal brine. Desalination energy of order 300 MW continuous is power-plant scale; the Phase II closed-loop geothermal network and regional solar resource can supply a fraction, but not all, of this load.

Honest status of the obstacles. Stage 2 removes the Panel's environmental objection and attaches a partial revenue stream (salt, gypsum, lithium) that did not exist in prior proposals, improving the cost calculus. It does *not* eliminate the multi-billion-dollar capital requirement, the multi-decade construction timeline, or the need for a bilateral treaty with Mexico; nor does it resolve where tens of millions of tonnes of recovered solids are placed each year. We present Stage 2 as a credible direction made newly admissible by brine-free ZLD desalination—not as a solved problem. The contribution of this paper is to establish Stage 1 as a concrete, independently beneficial first step on the Mexican side that proves the enabling chemistry, generates operating data, and earns the binational trust on which any Stage 2 treaty would depend.

Table 2: First-order Stage 2 budget for offsetting the Salton Sea net deficit (8×10^8 m^3/yr delivered freshwater) via hybrid conventional desalination with a brine-free ZLD backend. Figures are order-of-magnitude and intended to scope feasibility, not to specify a design.

Quantity	**Value**	**Basis / note**
Delivered freshwater (deficit offset)	8×10^8 m^3/yr	mid of 0.7–1.0 km^3/yr
Seawater feed (RO, 45% recovery)	1.8×10^9 m^3/yr	
Brine eliminated from marine discharge	$\sim 1.0 \times 10^9$ m^3/yr	now processed by ZLD
Salt recovered as solids	~ 60 Mt/yr	exceeds salt markets; disposal/use challenge
Lithium co-product (seawater grade)	~ 150 t/yr	$\gg$ if applied to geothermal brine
Desalination energy	~ 300 MW continuous	at 3.5 kWh/m^3; partly geothermal/solar
Capital cost, timeline, treaty	unresolved	IRP obstacles #1–#2 persist

5.2 Geothermal-Brine Lithium Co-Production: The Cost Lever

The lithium recoverable from the imported Gulf seawater is negligible at the scale of restoration (Section 4.1); the economically decisive lithium resource is the native geothermal brine of the Salton Sea Known Geothermal Resource Area—the "Lithium Valley" resource that the BTVP Phase II closed-loop network is positioned to access. Brine production from the existing geothermal field has averaged just over 1.2×10^8 metric tons per year since 2004, and at a conservative lithium concentration of ~ 200 mg/L this corresponds to on the order of 127,000 metric tons per year of contained lithium carbonate equivalent (LCE) [26, 27]. Measured concentrations range higher—up to ~ 400 mg/L in some wells [28]—and the total in-place reservoir resource is estimated at 4.1 million tons LCE in the well-characterized zone, rising to ~ 18 million tons under probable assumptions [26]. The same hydrogen-titanate selective-recovery chemistry demonstrated for seawater [13] applies directly to this far richer feedstock.

We model annual production as $\dot{m}_{LCE} = \xi\, Q_{brine}\, C_{Li}\, \eta_{Li}$, where Q_{brine} is brine volume throughput, C_{Li} the lithium concentration, η_{Li} the direct-lithium-extraction (DLE) recovery efficiency, and $\xi = 5.323$ the LCE-to-lithium-metal mass ratio. Taking a deliberately conservative *base technical case* of $C_{Li} = 200$ mg/L and $\eta_{Li} = 70\%$ at the existing throughput yields $\approx 74{,}500$ t/yr LCE (Appendix 8, Figure 7). At 2026 lithium prices—which have ranged from below \$14,000/t in late 2025 to nearly \$26,000/t in early 2026, against a 2022 peak above \$80,000/t [29]—this base case generates the revenues in Table 3, net of an assumed \$4,000/t DLE operating cost.

Table 3: Geothermal-brine lithium economics at the base technical case (200 mg/L, 70% recovery, $\approx$ 74,500 t/yr LCE), compared with the annualized cost of Stage 2 water delivery (capex \$30–150 B annualized at 30 yr, 5%; capital recovery factor 0.065, plus $\sim$\$0.5 B/yr O&M). Offset is the share of Stage 2 annual cost covered by net lithium revenue. Figures are order-of-magnitude.

Lithium price (\$/t LCE)	**Gross rev. (\$B/yr)**	**Net rev. (\$B/yr)**	**Offset of Stage 2 cost**
Trough, \$10,000	0.75	0.45	4%–18%
Base, \$20,000	1.49	1.19	12%–49%
Spike, \$30,000	2.24	1.94	19%–79%

Offset range spans high-capex (\$150 B) to low-capex (\$30 B) Stage 2 bounds.

Figure 8 plots gross lithium revenue against price for two brine grades, with the Stage 2 annualized-cost band overlaid; Figure 9 maps the share of the (optimistic, \$30 B-capex) Stage 2 cost offset across the price–recovery plane, with the 50% and 100% frontiers marked.

Honest reading of the economics. The result is materially favorable but not a panacea, and we state it as such. At the base technical case and 2026 prices, geothermal-lithium net revenue offsets roughly 12%–

49% of the annualized cost of Stage 2 water delivery—enough to move the project from clearly uneconomic toward partially self-financing, which is a qualitative change from the standalone import schemes the 2022 Panel rejected on cost grounds [2]. Full offset, however, is reached only under simultaneously optimistic assumptions: the break-even lithium price against the low-capex Stage 2 bound is ≈ \$37,000/t (and ≈ \$142,000/t against the high-capex bound)—both above prevailing 2026 levels. Three caveats bound the claim. First, lithium prices have swung threefold within single years, so any single-price projection is fragile; the case must be made on a price *distribution*, not a point estimate. Second, the DLE recovery η_{Li} at field scale on real multi-component brine remains unproven above pilot scale. Third, and importantly, the geothermal-lithium revenue is not unencumbered: it is already the basis of independent Lithium Valley commercial development, so hypothecating a share of it to fund Salton Sea water delivery is a policy and royalty-design choice, not a free input. The defensible conclusion is that lithium co-production makes a Stage 2 program *financeable in principle* in a way prior proposals were not—contingent on royalty policy, sustained prices, and demonstrated recovery—rather than that it pays for itself outright.

6 Conclusion

The Biotic–Thermal Vapor Pump reframes a long-standing but repeatedly rejected idea—importing Gulf of California water to address the Salton Sea crisis—as a physically constrained remediation-and-resource-recovery system rather than a water-importation or rain-making scheme. Its central contribution is to remove the brine-discharge obstacle that ended prior Sea-to-Sea review [2]: by substituting an unbuffered open evaporation pool with a managed halophytic canopy and an additive-free, brine-discharge-free solar-thermal evaporator, the system prevents the water-activity (a_w) collapse of hypersaline accumulation while recovering nearly all dissolved solids—including lithium—as solid product. Isolating the geothermal heat source within closed downhole loops eliminates the phreatomagmatic and hydrochloric-acid hazards of open injection while providing both process heat and access to the lithium-rich native brine. The pyrimidone MOST subsystem contributes temporal control over vapor release. Throughout, we have bounded each subsystem against the governing physics, and we have been explicit that the local atmospheric moisture return is a small, secondary effect rather than a basin-scale water-supply mechanism. Most importantly, we frame this design as Stage 1 of a two-stage program (Section 5): an independently beneficial remediation and resource-recovery installation on the Mexican side that proves the brine-free, zero-liquid-discharge desalination chain and thereby makes credible a Stage 2 in which the same technology—now answering the decisive environmental objection of the 2022 Independent Review Panel [2]—enables direct stabilization of the Salton Sea itself. Stage 1 is good for the Laguna Salada basin and for Mexico on its own terms; it is also the necessary, trust-building first step toward saving the Salton Sea.

References

[1] Pacific Institute. *Salton Sea Import/Export ("Sea-to-Sea") Plans*. Pacific Institute, Oakland, CA. `https://pacinst.org/salton-sea-import-export-plans/`

[2] Haddad, B. M. (lead author), Suri, R., Burgi, P., Glennon, R., Kenny, S. D., Lockwood, J., Paytan, A., Raucher, R. (2022). *Salton Sea Independent Review Panel Summary Report: Evaluation of Water Importation Concepts for Long-Term Salton Sea Restoration*. Institute for Social Transformation, University of California Santa Cruz, September 2022. `https://transform.ucsc.edu/publication/salton-sea-independent-review-panel-summary-report/`

[3] California Salton Sea Management Program (SSMP), California Natural Resources Agency, Department of Water Resources, and Department of Fish and Wildlife. *Improving Conditions at California's Salton Sea*. `https://saltonsea.ca.gov/`

[4] ScienceDaily. (2013). European Geosciences Union (EGU). "Could planting trees in the desert mitigate climate change?." ScienceDaily. ScienceDaily, 31 July 2013. `https://www.sciencedaily.com/releases/2013/07/130731093456.htm`

[5] Jiang and Sternberg et al. (2014). Bistability of mangrove forests and competition with freshwater plants. *Ecological Modelling.* https://doi.org/10.1016/j.agrformet.2014.10.004

[6] Adame, Lovelock and Reef (2020). Mangroves in arid regions: Ecology, threats, and opportunities *Estuarine, Coastal and Shelf Science.* https://doi.org/10.1016/j.ecss.2020.106796

[7] Qinwan Chong, et al. (2022). Evaluation of closed-loop U-Tube deep borehole heat exchanger in the Basal Cambrian Sandstone formation, Alberta, Canada *Geothermal Energy* https://link.springer.com/article/10.1186/s40517-022-00229-z

[8] UCSB Current (2026). UCSB scientists bottle the sun with liquid battery. https://news.ucsb.edu/2026/022384/ucsb-scientists-bottle-sun-liquid-battery

[9] New Atlas (2026). New molecular tech revolutionizes solar heat storage. https://newatlas.com/energy/sunlight-solar-energy-molecule-pyrimidone-ucsb/

[10] Nguyen, H., Han, G., Houk, K. (2026). DNA-Inspired Solar Energy Storage Using Modified Pyrimidone Structures for Molecular Solar Thermal (MOST) Technology. *Science* (As reported in ScienceDaily, May 2026).
https://www.sciencedaily.com/releases/2026/05/260513221821.htm

[11] Nguyen H.P.Q. et al. (2026). Molecular solar thermal energy storage in Dewar pyrimidone beyond 1.6 MJ/kg. *Science.* https://doi.org/10.1126/science.aec6413

[12] Tang, L., Singh, S. C., Wei, R., Xu, T., Guo, C. (2026). Additive-free and brine-discharge-free solar-thermal desalination with simultaneous complete mineral mining from ocean water. *Light: Science & Applications*, 15(1). https://doi.org/10.1038/s41377-026-02315-4

[13] Tang, L., Singh, S. C., Ma, M., Guo, C. (2026). Rapid lithium extraction via solar-thermal interfacial evaporation with zero liquid discharge. *Journal of Materials Chemistry A*, 14(25), 16023. https://doi.org/10.1039/D5TA08968A

[14] University of Rochester (2026). New method turns ocean water into drinking water, without waste. *University of Rochester News Center*, 27 May 2026.
https://www.rochester.edu/newscenter/what-is-desalination-definition-ocean-water-704732/

[15] Wentz, F. J., Ricciardulli, L., Hilburn, K., Mears, C. (2007). How Much More Rain Will Global Warming Bring? *Science*, 317(5835), 233–235.
https://doi.org/10.1126/science.1140746

[16] Fazle Rabbi et al. (2025). Middle Eastern mangroves at the arid limit (Red Sea and Arabian/Persian Gulf): eco-biophysical dynamics, blue-carbon MRV, climate-risk pathways, and governance for resilient restoration *Front. Mar. Sci., 30* https://doi.org/10.3389/fmars.2025.1695426

[17] Hannah R. Doran, et al. (2021). Modelling an unconventional closed-loop deep borehole heat exchanger (DBHE): sensitivity analysis on the Newberry volcanic setting *Geothermal Energy.* https://link.springer.com/article/10.1186/s40517-021-00185-0

[18] Mattox, T. N., Mangan, M. T. (1997). Littoral hydrovolcanic explosions: a case study of lava–seawater interaction at Kilauea Volcano. *Journal of Volcanology and Geothermal Research*, 75, 1–17.
https://volcanoes.usgs.gov/vsc/file_mngr/file-186/Mattox%20and%20Mangan_hydrovolcanic%20explosions.pdf

[19] Rosenfeld et al. (2023). Rethinking water security: rainfall enhancement. *npj Climate and Atmospheric Science.* https://www.nature.com/articles/s41612-023-00503-2

[20] Minder and Roe (2010). Orographic Precipitation. Encyclopedia of Atmospheric Sciences. https://earthweb.ess.washington.edu/roe/GerardWeb/Publications_files/MinderRoe_OrogPrecEncyc.pdf

[21] Kirshbaum et al. (2018). Moist Orographic Convection. *Atmosphere, 9(3), 80.* https://doi.org/10.3390/atmos9030080

[22] Flossmann et al. (2019). Review of Advances in Precipitation Enhancement Research. *BAMS, 100(8).* https://doi.org/10.1175/BAMS-D-18-0160.1

[23] Paltrinieri, D., Favali, P., et al. (2022). The Marsili Seamount Offshore Geothermal Reservoir: A Big Challenge for an Energy Transition Model. *Energies*, 15(5), 1900. https://doi.org/10.3390/en15051900

[24] Pegler, S. S., Ferguson, D. J. (2021). Rapid heat discharge during deep-sea eruptions generates megaplumes and disperses tephra. *Nature Communications*, 12, 2292. https://doi.org/10.1038/s41467-021-22439-y https://www.syfy.com/syfy-wire/could-underwater-volcanoes-deliver-energy-needs

[25] Earth Science StackExchange. (2018–2022). *Is it possible to create clouds by pumping water into volcanoes?* (Commentary and analyses by Trond Hansen, Victor, Gimelist, MartyS, and userLTK). https://earthscience.stackexchange.com/questions/14822/is-it-possible-to-create-clouds-by-pumping-w

[26] Lawrence Berkeley National Laboratory / U.S. Department of Energy (2023). *Characterizing the Geothermal Lithium Resource at the Salton Sea.* Estimates ∼127,000 t/yr LCE contained in produced brine at ∼198 ppm, and a 4.1–18 million t LCE in-place reservoir resource. https://eta.lbl.gov/publications/characterizing-geothermal-lithium

[27] National Renewable Energy Laboratory (2021). *Lithium-Extraction Resource Assessment for Geothermal Brines* (NREL/TP-5700-79178). Reports ∼121 Mt/yr Salton Sea brine throughput (CalGEM 2019) and ∼200 mg/L Li (McKibben & Hardie 1997). https://docs.nrel.gov/docs/fy21osti/79178.pdf

[28] SRI International / California Energy Commission (2020). *Selective Recovery of Lithium from Geothermal Brines* (CEC-500-2020-020). Reports Salton Sea KGRA brine Li concentrations up to ∼400 mg/L. https://www.energy.ca.gov/sites/default/files/2021-05/CEC-500-2020-020.pdf

[29] Investing News Network (2026). *Lithium Price Forecast and Market Update.* Battery-grade lithium carbonate rebounded from below $14,000/t (late 2025) to ∼$26,000/t (early 2026), against a 2022 peak above $80,000/t. https://investingnews.com/daily/resource-investing/battery-metals-investing/lithium-investing/lithium-forecast/

[30] Frederick Pontius (2018) *Treatability of a Highly-Impaired, Saline Surface Water for Potential Urban Water Use* Water 2018, 10(3), 324; https://doi.org/10.3390/w10030324

7 Appendix: Transient Basin Hydrochemistry and Box Model Specifications

This appendix provides the computational specifications and architectural breakdowns for the transient simulation suite used to derive the 40-year remediation horizon profiles shown in Section 4. The complete modeling architecture is executed via an explicit forward-Euler finite difference scheme with a temporal mesh step of $\Delta t = 0.01$ years.

7.1 Mathematical Model Framework

The programmatic architecture tracks four core physical vectors across time: liquid volume (V), total dissolved salt mass (S), instantaneous concentration (C), and cumulative dry-mass salt extraction ($M_{\text{extracted}}$).

The state transitions are updated at each iteration step n according to the following discrete structures:

$$V^{n+1} = V^n + \left[Q_{\text{in}} - E_{\text{nat}} \cdot 900 \left(\frac{V^n}{7.5} \right)^{0.68} - Q^n_{\text{plant}} (1 - Y_{\text{ro}}) \right] \Delta t \tag{4}$$

$$S^{n+1} = S^n + \left[Q_{\text{in}} C_{\text{in}} - Q^n_{\text{plant}} C^n \eta_{\text{rejection}} \right] \Delta t \tag{5}$$

$$C^{n+1} = \frac{S^{n+1}}{V^{n+1}} \tag{6}$$

$$M^{n+1}_{\text{extracted}} = M^n_{\text{extracted}} + \left[Q^n_{\text{plant}} C^n \eta_{\text{rejection}} \right] \Delta t \tag{7}$$

7.2 Ecosystem Optimization Figures and Descriptions

The dynamic interaction of these parameters produces two key performance visualizations required for infrastructure scaling, included below:

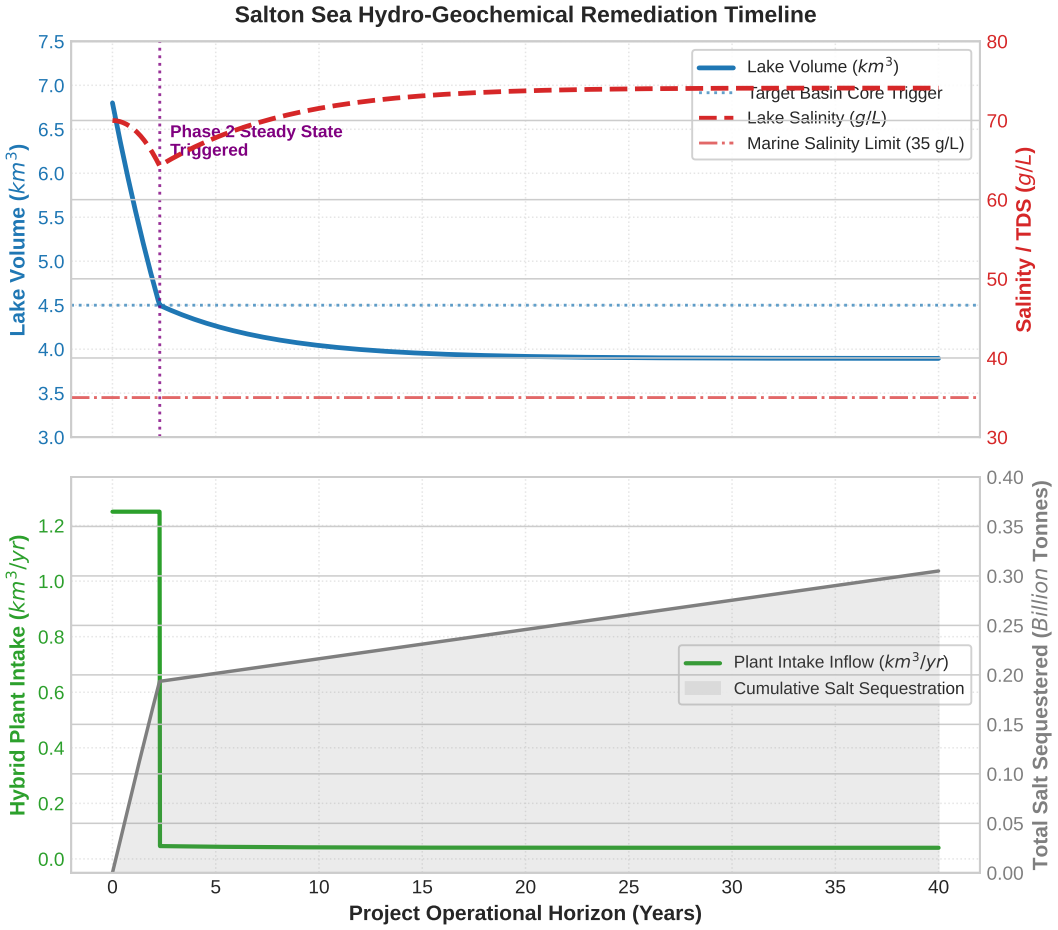

Figure 5: Transient hydro-geochemical remediation timeline of the Salton Sea under a salt-mass balance priority framework. Phase 1 shows high-throughput stripping of legacy salt mass over the first 2.3 years, followed by automated throttling into Phase 2 maintenance mode to lock the basin permanently at marine-equivalent salinity (35 g/L).

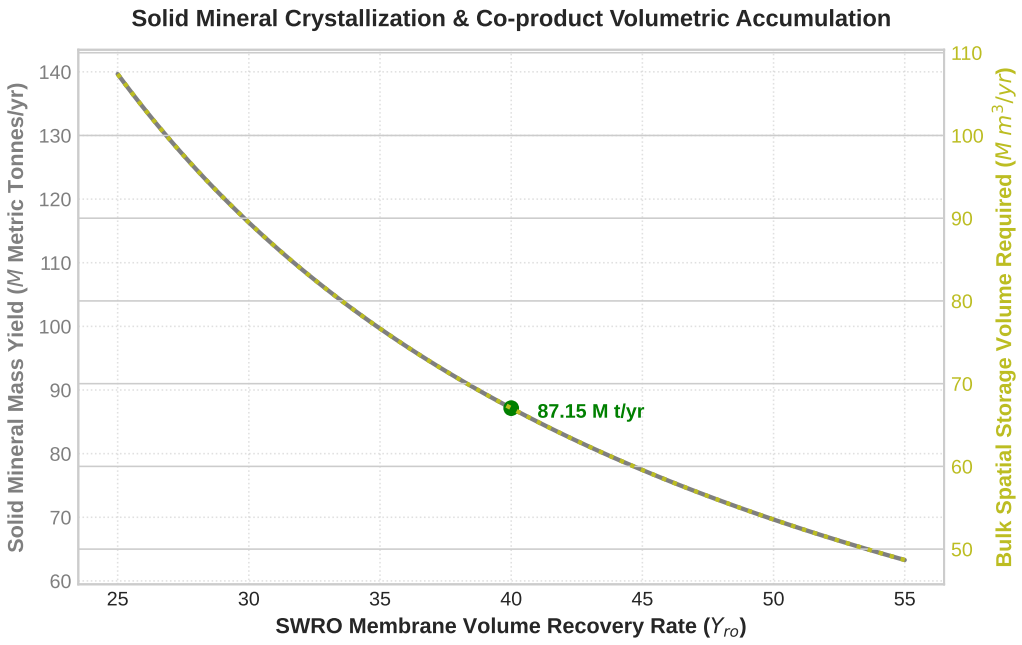

Figure 6: Long-term solid mineral co-product crystallization yield and spatial storage requirements. The highlighted design locus marks the steady-state operating horizon where the system permanently manages the continuous agricultural salt influx, avoiding brine back-discharge loops.

7.3 Interpretation of Performance Profiles

As plotted in Figure 5, the system initiates a sharp, high-velocity cleanup phase (Phase 1) during the first 2.29 years, drawing down the hyper-saline water table and processing the raw legacy burden. The sudden structural inflection point occurs when the automated controller detects that the basin volume is reaching its stabilized threshold.

Rather than executing a complete infrastructure shutdown—which triggers the immediate salinity rebound outlined in Section 4.2—the system seamlessly dials down the intake from $1.25\,\mathrm{km}^3$/yr to the continuous salt-balancing baseline. Figure 6 quantifies the exact physical outputs generated by this continuous loop. Throughout the 40-year project lifetime, the BTVP solid-phase processor safely crystallizes and isolates an aggregated total of ~ 1.22 Billion Metric Tonnes of solid salt compounds from the water column, validating the scale-dependent utility of the superwicking evaporative surfaces under real-world basin impairments.

8 Appendix: Computational Methods and Economic Sensitivity

All source code used in this paper is available at: `https://github.com/brentharts/saltonsea`
The quantitative bounds in this paper are reproduced by two short, self-contained Python scripts provided as supplementary material: `scale.py` (solar energy budget, evaporator manufacturing throughput, and MOST energy fraction, Section 3.2 and Table 1) and `lithium_economics.py` (geothermal-brine lithium production and Stage 2 cost offset, Section 5.2 and Table 3). Each prints its input assumptions and intermediate quantities so that results can be audited and re-run under alternative parameters.

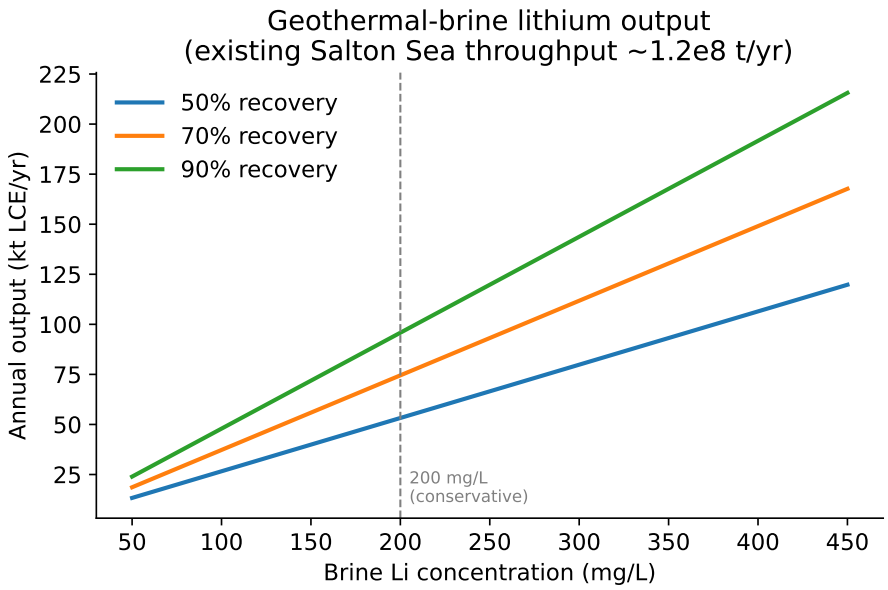

Figure 7: Annual geothermal-brine lithium output (kt LCE/yr) as a function of brine lithium concentration, for three DLE recovery efficiencies, at the existing Salton Sea field throughput ($\sim 1.2\times10^8$ t/yr). The dashed line marks the conservative 200 mg/L assumption.

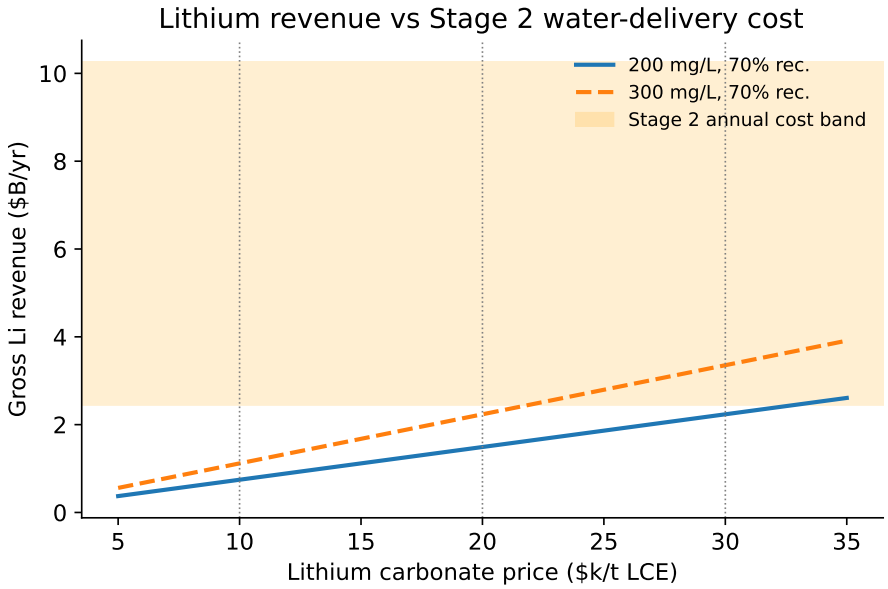

Figure 8: Gross lithium revenue versus lithium carbonate price for two brine grades (70% recovery), with the annualized Stage 2 water-delivery cost band (capex \$30–150 B) shaded. Dotted lines mark the trough/base/spike price scenarios of Table 3.

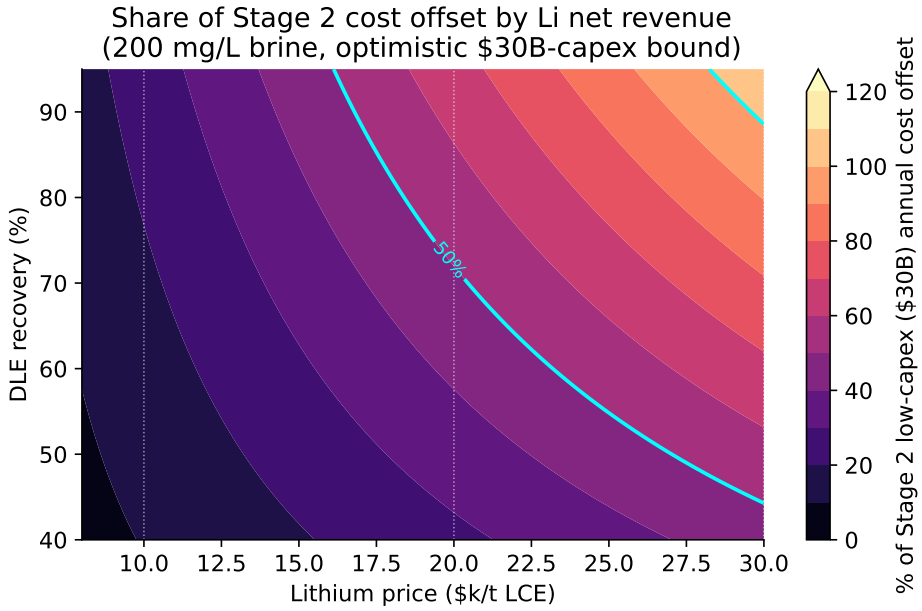

Figure 9: Share of the optimistic ($30 B-capex) Stage 2 annualized cost offset by net lithium revenue across the price–recovery plane, at 200 mg/L brine. Cyan contours mark the 50% and 100% offset frontiers; full offset of even the low-capex bound requires simultaneously high price and high recovery.